doi:10.1093/brain/awv408 BRAIN 2016: 139; 1237–1251 | 1237

BRAIN
A JOURNAL OF NEUROLOGY

Regulatory T cells delay disease progression in Alzheimer-like pathology

Cira Dansokho,[1,2,*] Dylla Ait Ahmed,[1,2,*] Saba Aid,[2,3,*] Cécile Toly-Ndour,[1,2,*] Thomas Chaigneau,[1,2] Vanessa Calle,[1,2] Nicolas Cagnard,[4] Martin Holzenberger,[2,3] Eliane Piaggio,[5,6] Pierre Aucouturier[1,2] and Guillaume Dorothée[1,2]

*These authors contributed equally to this work.

Recent studies highlight the implication of innate and adaptive immunity in the pathophysiology of Alzheimer's disease, and foster immunotherapy as a promising strategy for its treatment. Vaccines targeting amyloid-β peptide provided encouraging results in mouse models, but severe side effects attributed to T cell responses in the first clinical trial AN1792 underlined the need for better understanding adaptive immunity in Alzheimer's disease. We previously showed that regulatory T cells critically control amyloid-β-specific $CD4^+$ T cell responses in both physiological and pathological settings. Here, we analysed the impact of regulatory T cells on spontaneous disease progression in a murine model of Alzheimer's disease. Early transient depletion of regulatory T cells accelerated the onset of cognitive deficits in APPPS1 mice, without altering amyloid-β deposition. Earlier cognitive impairment correlated with reduced recruitment of microglia towards amyloid deposits and altered disease-related gene expression profile. Conversely, amplification of regulatory T cells through peripheral low-dose IL-2 treatment increased numbers of plaque-associated microglia, and restored cognitive functions in APPPS1 mice. These data suggest that regulatory T cells play a beneficial role in the pathophysiology of Alzheimer's disease, by slowing disease progression and modulating microglial response to amyloid-β deposition. Our study highlights the therapeutic potential of repurposed IL-2 for innovative immunotherapy based on modulation of regulatory T cells in Alzheimer's disease.

1 INSERM, UMRS 938, CdR Saint-Antoine, Laboratory Immune System, Neuroinflammation and Neurodegenerative Diseases, Hôpital St-Antoine, F-75012, Paris, France
2 Sorbonne Universités, UPMC Univ Paris 06, UMRS 938, CdR Saint-Antoine, Hôpital Saint-Antoine, F-75012, Paris, France
3 INSERM, UMRS 938, CdR Saint-Antoine, Laboratory Neuroendocrine mechanisms of longevity and age-related diseases, Hôpital St-Antoine, F-75012, Paris, France
4 Bioinformatics Platform, Faculty of Medicine Paris Descartes, Hôpital Necker-Enfants Malades, F-75015 Paris, France
5 INSERM, U932, Institut Curie, Section Recherche; Center of Clinical Investigation (CIC-BT-507), F-75005, Paris, France
6 Sorbonne Universités, UPMC Univ Paris 06, CNRS, UMR7211, Immunology-Immunopathology-Immunotherapy, F-75013 Paris, France

Correspondence to: Dr Guillaume Dorothée,
INSERM UMRS 938,
Laboratory 'Immune System,
Neuroinflammation and Neurodegenerative diseases',
Hôpital Saint-Antoine,
184 rue du Faubourg Saint-Antoine,
F-75012, Paris,
France
E-mail: guillaume.dorothee@inserm.fr

Received June 18, 2015. Revised November 18, 2015. Accepted November 23, 2015. Advance Access publication February 1, 2016

Keywords: Alzheimer's disease; regulatory T cells; microglia; immunotherapy

Abbreviations: IFN = interferon; Teffs = effector T cells; Tregs = regulatory T cells

Introduction

Alzheimer's disease is a neurodegenerative disorder characterized by progressive loss of memory and cognitive functions. Neuropathological features include extracellular deposits of amyloid-β peptide, intraneuronal neurofibrillary tangles, and chronic neuroinflammation associated with astrocytosis and microgliosis. Active immunization against amyloid-β proved efficient at preventing amyloid-β deposition and reversing cognitive deficits in murine models of the disease (Schenk *et al.*, 1999; Janus *et al.*, 2000; Morgan *et al.*, 2000). Subsequent AN1792 clinical trial of amyloid-β vaccination was halted after the occurrence of meningoencephalitis in 6% of vaccinated patients. These severe side effects were attributed to vaccine-induced T cell responses, suggesting a detrimental role of amyloid-β-specific T cells in the context of Alzheimer's disease (Nicoll *et al.*, 2003; Orgogozo *et al.*, 2003; Ferrer *et al.*, 2004). Later reports in mouse models of the disease suggested that $CD4^+$ T cells might be either detrimental or beneficial depending on the effector type. Whereas vaccine-induced Th1 cells specific for amyloid-β may promote both enhanced amyloid-β clearance and encephalitis (Monsonego *et al.*, 2006), Th2 cells specific for amyloid-β reverse cognitive decline and synaptic loss in mice with Alzheimer-like pathology (Ethell *et al.*, 2006; Cao *et al.*, 2009). Accumulating evidence also suggest an implication of spontaneous $CD4^+$ T cell responses in the pathophysiology of Alzheimer's disease. Genome-wide association studies identified MHC-II-associated polymorphisms as new susceptibility loci for Alzheimer's disease (Jones *et al.*, 2010; Lambert *et al.*, 2010, 2013). These data are in line with previous studies describing increased intracerebral T cell infiltration and enhanced peripheral $CD4^+$ T cell responses to amyloid-β in patients suffering from Alzheimer's disease (Togo *et al.*, 2002; Monsonego *et al.*, 2003). Together, these studies suggest a complex implication of $CD4^+$ T cells in the disease, with multiple outcomes that depend on magnitude and functionality of T cell responses at different disease stages.

$CD4^+CD25^+Foxp3^+$ regulatory T cells (Tregs) are key modulators of immune responses, which play a critical role in maintaining immunological tolerance to self-antigens and in suppressing excessive immune responses deleterious to the host (Sakaguchi *et al.*, 2008). Tregs were suggested to play a beneficial role in the pathophysiology of various neurodegenerative disorders, including Parkinson's disease and amyotrophic lateral sclerosis (Reynolds *et al.*, 2010; Beers *et al.*, 2011). The impact of Tregs in Alzheimer's disease is poorly understood, and conflicting results have been reported. Previous studies suggested increased suppressive activity in patients as compared to non-demented controls (Rosenkranz *et al.*, 2007). In contrast, overall decreased frequency of $CD4^+CD25^{hi}$ T cells and altered naive/memory ratio within this population were described in patients with mild Alzheimer's disease as compared to age-matched controls (Larbi *et al.*, 2009). Other studies reported that a highly suppressive $PD1^-$ Treg subpopulation was enhanced in mild cognitive impairment but not in patients with severe Alzheimer's disease, and Treg-mediated suppression was more efficient in mild cognitive impairment as compared to severe patients and healthy controls (Saresella *et al.*, 2010). In a mouse model of Alzheimer's disease, we previously suggested that Tregs critically control the magnitude of $CD4^+$ T cell responses to amyloid-β in Alzheimer-like pathology and in response to amyloid-β vaccination. Importantly, the potency of such Treg-mediated inhibition of $CD4^+$ T cells specific for amyloid-β strongly vary according to genetic backgrounds, suggesting that intrinsic genetic variations among individuals may result in differential modulation by Tregs of the pathogenesis of Alzheimer's disease and/or response to amyloid-β vaccination (Toly-Ndour *et al.*, 2011). Altogether, these results suggest an implication of Tregs in the pathophysiology of Alzheimer's disease, but their actual impact on disease progression remains unknown.

In this study, we investigated the role of Tregs in the pathophysiology of the disease independently of vaccination. Using the APPPS1 mouse model, we show that depletion of Tregs accelerates the onset of cognitive deficits triggered by amyloid-β deposition. Such early cognitive impairment is associated with reduced recruitment of microglia towards amyloid deposits and altered disease-related gene expression profile in the brain. Conversely, selective amplification of Tregs by low-dose IL-2 treatment increases numbers of plaque-associated microglia, and improves cognitive functions in APPPS1 mice.

Materials and methods

Experimental design

The aim of the study was to investigate the impact of Tregs on spontaneous disease progression in a murine model of Alzheimer-like pathology. APPPS1 mice and littermate controls were used in all experiments, which aimed at analysing the effect on cognitive functions and neuropathology of either depletion or amplification of Tregs. Depletion was induced by intraperitoneal injection of anti-CD25 antibody (clone PC61), whereas amplification of Tregs was achieved by low-dose IL-2 treatment administered either transiently

or chronically. Mice of each genotype were randomly assigned to treatment groups. Separate cohorts of animals were treated in parallel and dedicated to behaviour studies, neuropathological studies or gene array analysis. Effects of treatments on the frequency of Tregs and other immune populations were confirmed by flow cytometry. Cognitive functions were assessed using the Barnes maze test. The Y-maze test was additionally carried out to further assess the impact on cognitive functions after amplification of Tregs. Impact on neuropathology was analysed by immunohistochemistry, ELISA assays, and transcriptome analysis. All behaviour studies and quantifications for neuropathological assessment were carried out blindly. Sample sizes were chosen based on previous experience and similar type of studies previously described by others. Detailed study design and sample sizes are described in Supplementary Tables 1 and 2.

Mice

APPPS1 transgenic mice (Thy1-APP$^{KM670/671NL}$; Thy1-PS1^{L166P}) on C57BL/6 background were kindly provided by Prof. Mathias Jucker (Hertie Institute for Clinical Brain Research, University of Tübingen, Tübingen, Germany) and maintained by breading heterozygotes with wild-type C57BL/6j mice. Animals were kept under strictly monitored specific and opportunistic pathogen-free conditions. All experimental protocols involving animal studies have been approved by the Charles Darwin Ethical Committee for Animal Studies, and were carried out in compliance with European legislation on animal care and scientific experimentation.

Treg depletion or amplification

For Treg depletion, 4–5-week-old APPPS1 mice and wild-type littermates were injected intraperitoneally with 200 µg of either purified (BioXCell) or ascite-derived anti-CD25 depleting monoclonal antibody (clone PC61) diluted in phosphate-buffered saline (PBS). Control mice were injected with either PBS or 200 µg of purified control IgG1 (BioXCell). Similar treatments were repeated 4 weeks after the first injection. For amplification of Tregs, 6-week-old APPPS1 mice and wild-type littermates were treated daily for 10 consecutive days with intraperitoneal injections of either PBS or 50 000 IU of recombinant human IL-2 (Proleukin; Novartis) diluted in PBS. Additional daily treatments for 5 days were repeated every 3 weeks.

Flow cytometry analysis

The efficiency of treatments for Treg depletion or amplification was monitored by flow cytometry using a combination of surface and intracellular staining. For depletion studies, efficiency was evaluated by quantifying Tregs in the blood the day before injection and 6–7 days following each round of PC61 treatment. Efficiency of IL-2 treatment was monitored in a pilot cohort by quantifying Tregs in the blood, spleen and cervical lymph nodes the day before the first injection, and 4, 8 and 11 days after. In all studies cells were first incubated with Fc receptor blocking antibody (2.4G2; BD Biosciences) to avoid non-specific staining. PE-Cy5-conjugated anti-TCRβ (H57-597), FITC-conjugated anti-CD4 (L3T4), biotinylated anti-CD25 (7D4) and APC-conjugated streptavidin (all from BD Biosciences) were used for cell-surface staining. For intranuclear staining, cells were then fixed, permeabilized and incubated with PE-conjugated anti-Foxp3 (FJK-16 s; eBioscience) according to the manufacturer's specifications. Fluorescence data were collected on a LSRII flow cytometer (BD Biosciences) and analysed using Flowjo software (Tree Star, Inc.).

DNA microarray analysis

At 4 and 8 weeks of age, wild-type and APPPS1 mice received an intraperitoneal injection of PBS or 200 µg of anti-CD25 monoclonal antibody (clone PC61). Brains were harvested at 4 months of age after transcardiac perfusion with PBS. Cerebellum was removed and total RNA was extracted from hemi-brains using RNeasy® lipid tissue midi kit (Qiagen). Following DNase treatment, RNA quality was verified using an Agilent Bioanalyzer and quantity measured with a Nanodrop 1000 (ThermoFisher Scientific). Total RNA was amplified and converted to biotinylated cRNA according to the manufacturer's protocol (Illumina® TotalPrep™ RNA Amplification Kit; Ambion). Microarray experiments were performed on mouse genome-wide array (WG6 BeadChip, Illumina) comprising 45 282 probes. Data were extracted and Quantile normalized using BeadStudio software (Illumina). Each dataset was derived from three biologically independent replicate samples. The working lists were created by filtering probes with detection $P < 0.05$ for at least half of the chips involved in the comparison. Independent samples were compared by two-tailed unpaired Student's *t*-test filtered at $P < 0.05$ and by amplitude of expression modulation at a threshold assessed on the variations of the background-flagged probes. Cluster analysis was performed by hierarchical clustering using the Spearman correlation similarity measure and average linkage algorithm. Data were submitted to Ingenuity Pathway Analysis (http://www.ingenuity.com) to model relationships among genes and proteins and to construct pathways and unveil relevant biological processes.

Real-time quantitative PCR

Total RNA was prepared as described for microarray analysis and 2 µg used for cDNA synthesis using RT^2 First Strand kit. Quality control of RNA and cDNA samples was assessed using RT^2 RNA QC PCR Array. Relative expression of specific mRNAs was assessed by SYBR® green-based real time quantitative PCR using RT^2 qPCR Master Mix and ABI 7900HT light cycler (Applied Biosystems). All primers were from validated RT^2 qPCR Primer Assays. Amplification conditions were: 95°C for 10 min, then 40 cycles at 95°C for 15 s and 60°C for 1 min. A melting curve was generated at the end of amplification cycles for evaluating the specificity of the reaction. Peptidylprolyl isomerase A (*Ppia*) was used as a reference housekeeping gene for normalization. All reagents (RT^2 series) used for gene expression analysis were from Qiagen-SA Biosciences. Data were analysed using SDS.2.4 software (Applied Biosystem), Microsoft Excel and GraphPad Prism® software.

Amyloid-β ELISA

To assess amyloid-β_{1-42} levels, mouse hemi-brains were homogenized at 4°C in Tris buffer (50 mM Tris base pH 7.4, 250 mM sucrose, 1 mM EDTA, 1 mM EGTA, 1 mM $NaVO_3$, 10 mM NaF; 100 mg tissue per ml) with protease inhibitors (Roche) using a Polytron. Soluble and insoluble amyloid-β was extracted in 0.4% diethylamine and 70% formic acid, respectively. Briefly, crude 10% homogenate was mixed with an equal volume of 0.4% diethylamine, sonicated, and spun for 1 h at 4°C at 130 000 *g* using a TLA 50.4 Ti rotor and Optima TL ultracentrifuge (Beckman Coulter). The diethylamine supernatant was neutralized with 0.5 M Tris base (pH 6.8) and the pellet was homogenized in 70% formic acid, again ultracentrifuged, and formic acid-containing supernatants neutralized with 1 M Tris base (pH 11). Levels of amyloid-β_{1-42} were quantified using anti-human amyloid-β ELISA (Life Technologies), according to the manufacturer's instructions.

Immunohistochemistry

Mice were anaesthetized with ketamine (Imalgene®) and xylazine (Rompun™) in 0.9% NaCl solution, then transcardially perfused with ice-cold PBS, followed by a solution of 4% paraformaldehyde in PBS. Brain was harvested, transferred for 48 h at 4°C in a fresh solution of 4% paraformaldehyde, and transferred overnight at 4°C in 30% sucrose/PBS solution. After bisecting along the midline, each hemi-brain was divided into anterior, median and posterior parts by coronal sectioning. Each part was embedded individually in Optimal Cutting Temperature (O.C.T.; WVR) mounting medium, frozen in liquid nitrogen and stored at −80°C. Cryosections (7 µm) were prepared from median parts of the brain, using a Leica RM2145 cryostat, and mounted on SuperFrost™ Plus glass slides. At least three non-adjacent sections (100-µm apart) were labelled for each mouse. Sections were first rinsed in PBS, blocked with PBS–5% BSA–0.05% Tween 20 for 1 h at room temperature, and then incubated either overnight at 4°C with rabbit anti-Iba1 antibody (1/200) (Wako) or for 30 min at room temperature with rabbit anti-GFAP antibody (1/200) (Dako). Following three washes in PBS–0.1% BSA, sections were incubated for 30 min at room temperature with mouse anti-amyloid-β monoclonal antibody (1/200) (BAM10; Thermo Scientific), washed three times, and incubated for 30 min at room temperature with Alexa Fluor® 488-conjugated goat anti-rabbit and Alexa Fluor® 594-conjugated goat anti-mouse antibodies (1/1000 each) (Life Technologies). After three washes brain sections were stained with DAPI (1 µg/ml in PBS) and coverslipped with Immu-Mount™ medium (ThermoShandon). Double staining with anti-amyloid-β plus rabbit anti-CD68 (clone FA-11; Biolegend) or rabbit anti-KHDRBS1/SAM68 (Proteintech Group Inc.) was performed in the same way, except that all blocking, incubation and washing steps were carried out in the additional presence of 0.3% Triton™ X-100.

Microscopy and image analysis

For each mouse, three non-adjacent sections were imaged using an Olympus BX61 microscope equipped with an Olympus DP71 camera. Four random images of the cortex and one image for the hippocampus were collected at 20 × magnification for each section. All sections were immunostained and imaged using the same parameters. Quantifications were carried out by postprocessing images with the ImageJ software (http://rsbweb.nih.gov/ij). Percentage of specifically stained area was determined after standardized binarization of fluorescence images. For quantification of microglia recruitment towards amyloid deposits, we first delineated the proximal surrounding area for each amyloid-β deposit, which was defined as the limit encompassing twice the radius of the deposit. Amount of Iba1 or CD68 staining within this limit, i.e. corresponding to activated microglia co-localizing with or in close proximity to amyloid-β deposits, was determined from the binarized images. Pooled data from 4–6 mice/group were analysed, corresponding to at least $n > 90$ deposits of each size category.

Behaviour studies

Barnes maze

The Barnes maze is a spatial learning and memory task based on the natural preference of mice for dark closed environments over bright open areas. The maze consists of an elevated flat circular platform with 20 circular holes located equidistantly at the periphery of the platform. A hidden box located under one target hole allows the mice to escape from the platform. Fixed visual cues are displayed on distant walls around the maze for mice orientation. The test consisted of 4 days of learning, followed by one probe assay on Day 5 with the escape box being removed. Each mouse was given four trials per day during the learning phase and a single trial for the probe test. For each trial, mice were placed in an opaque start box located in the centre of the maze, ensuring a random starting orientation for each trial. After being released from the start box, mice were allowed to freely explore the maze for a maximum of 300 s (learning phase) or 90 s (probe assay). Indirect light and background noise (10 kHz, 75 dB) was used as a reinforcement to motivate the mice for escaping the maze. The trial was stopped when the mouse found the target hole or when the maximum duration of the trial was reached. Mice that did not find the escape box within 300 s of the learning trial were gently picked up and moved to the target hole, into the escape box. Mice were left in the escape box for 2 min before being returned to their home cage. The platform surface was carefully cleaned with 70% ethanol solution between each trial to remove any olfactory cues. An overhead video camera and automated video tracking software (Viewer^3 BIOBSERVE) were used for recording and analysing each behaviour trial. Numbers of errors, accuracy, path length and escape latency to reach the target hole were monitored. Accuracy was calculated as the sum of scores assigned to each hole visited by the mouse, with a score of zero being assigned to target hole, one to adjacent holes, and so forth towards the opposite hole that was assigned the highest score of 10; hence, the higher the score, the lower the accuracy.

Y-maze

The two-trial Y-maze task is based on rodents' preference for exploring novel areas over familiar ones, and has been suggested to measure several aspects of spatial working memory.

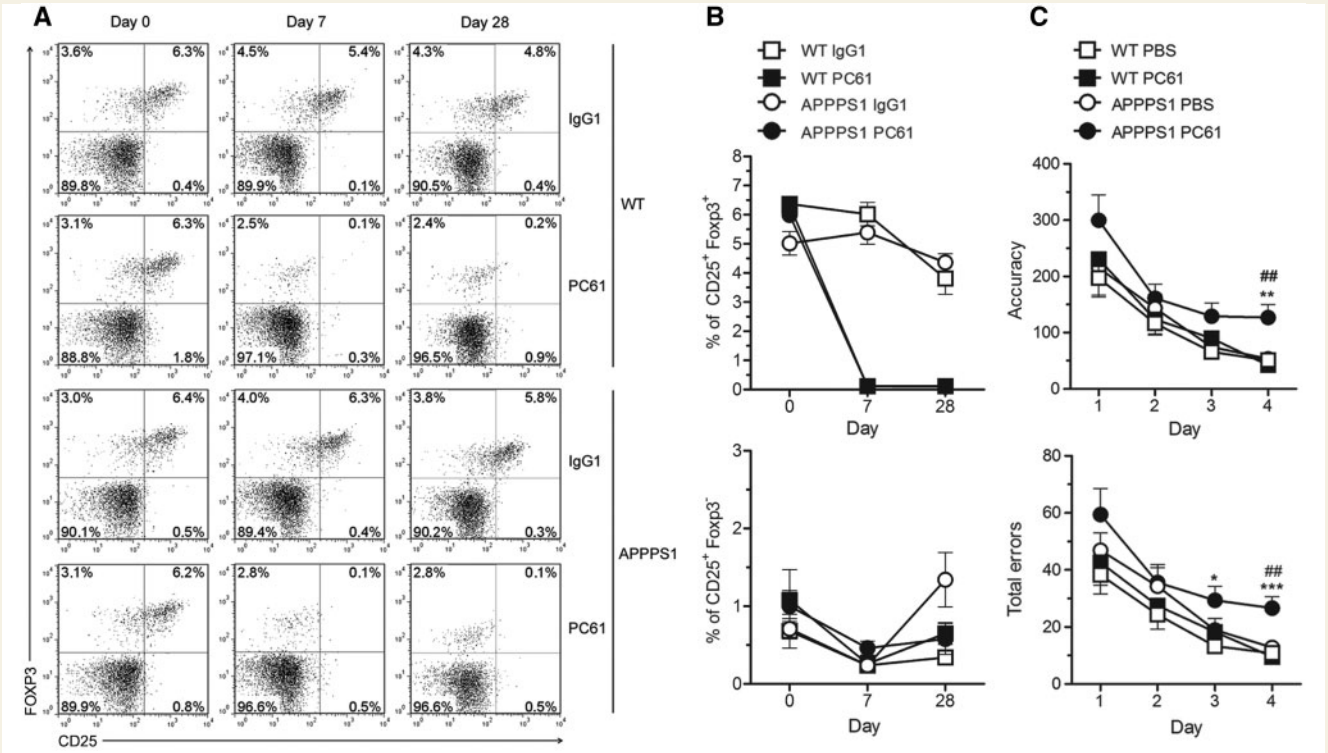

Figure 1 Early depletion of Tregs accelerates the onset of cognitive deficits in APPPS1 mice. Four- to 5-week-old APPPS1 mice and wild-type (WT) littermates were injected intraperitoneally with 200 μg of anti-CD25 antibody (PC61) and treatment was repeated 4 weeks later. Controls were injected with either PBS or 200 μg of control IgG1 antibody. (**A** and **B**) Frequency of $CD4^+CD25^+Foxp3^+$ Tregs and $CD4^+CD25^+Foxp3^-$ Teffs was evaluated in the blood by flow cytometry before (Day 0) and after initiating the treatment (Day 7, Day 28). (**A**) Representative flow cytometry plots gated on $CD4^+$ T cells. (**B**) Percentages of $CD25^+Foxp3^+$ Tregs and $CD25^+Foxp3^-$ Teffs among $CD4^+$ T cells. Mean ± SEM (n = 4–7 mice/group). Data representative of three independent experiments. (**C**) Impact of transient Treg cell depletion on spatial learning abilities of 7-month-old wild-type and APPPS1 mice, using the Barnes maze test. Accuracy and total errors to reach the target hole during the learning phase are shown. Mean ± SEM (n = 10–11 mice/group). Repeated measures ANOVA. $^*P < 0.05$, $^{**}P < 0.01$, $^{***}P < 0.001$ versus wild-type PBS; $^{\#\#}P < 0.01$ versus APPPS1 PBS.

The maze consists of three transparent plastic arms, 39 × 8 × 16 cm each, set at 120° angle relative to each other. During the first trial, mice could freely explore two arms ('start' arm and 'other' arm) for 5 min, while the third ('novel') arm was blocked with an opaque door. Assignment of arms was counterbalanced randomly within each experimental group to avoid any preference-related bias. Mice were then returned to their home cage for 2 min. During the second trial, mice were placed at the extremity of their start arm and allowed to explore all three arms for 2 min. The maze was carefully cleaned with 70% ethanol solution between each exploration phase to remove any olfactory cues. The Viewer3 BIOBSERVE Tracking System was used for recording and analysing each exploration trial. Latency to reach 'other arm' and 'novel arm' was monitored.

Statistics

All statistical analyses were carried out using Graphpad Prism version 6.0, SPSS software (IBM) and the R software for Statistical Computing (http://www.r-project.org/). Statistical tests included repeated measures ANOVA, Mann-Whitney non-parametric test and unpaired Student's t-test. The specific tests used in each experiment are mentioned in the figure legends. Non-significant P-values < 0.1 were provided for information.

Results

Transient early depletion of Tregs accelerates the onset of cognitive deficits in APPPS1 mice

We analysed the impact of Treg depletion on disease progression in APPPS1 mice, which start developing amyloid plaques at 6–8 weeks of age. $CD4^+CD25^+$ Tregs were transiently depleted at early disease stages by intraperitoneal injection of anti-CD25 antibody (PC61) at 4–6 weeks of age, followed by a second injection 4 weeks later. Each PC61 injection resulted in depletion of $CD4^+CD25^+Foxp3^+$ Tregs for up to 28 days, whereas frequency of $CD4^+CD25^+Foxp3^-$ effector T cells (Teffs) was not significantly affected (Fig. 1A and B). The impact of early Treg depletion on the development of cognitive deficits was evaluated by the Barnes maze test at 7

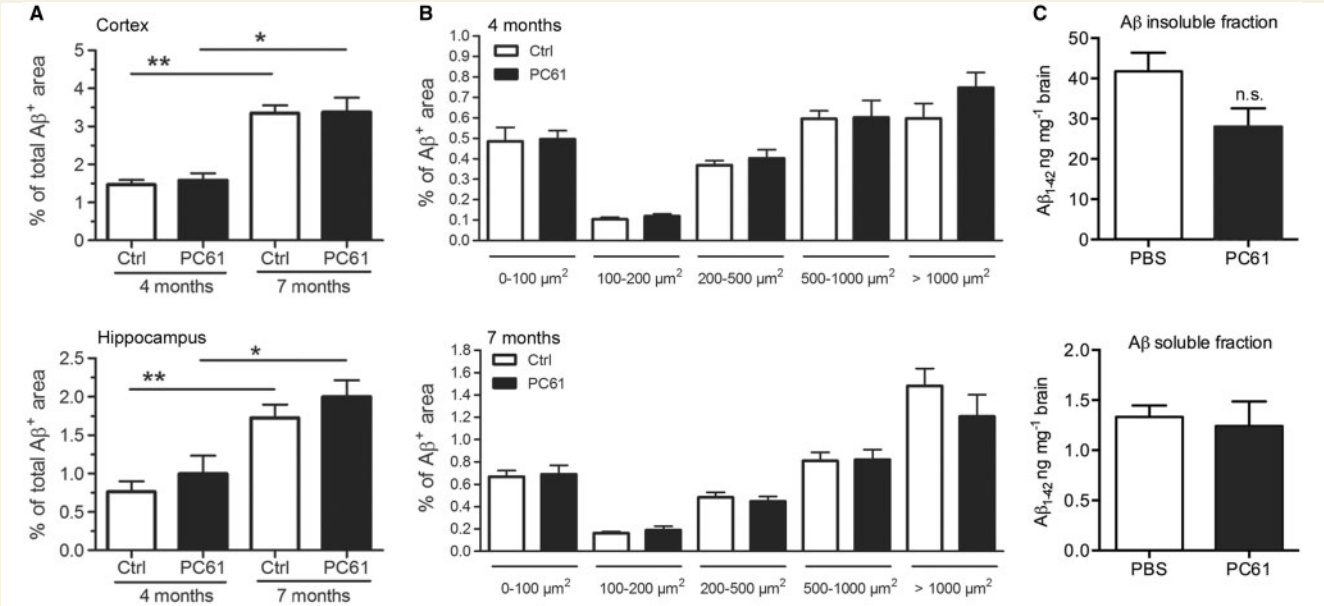

Figure 2 Treg cell depletion does not alter amyloid-β deposition in the brain of APPPS1 mice. (**A** and **B**) Immunohistochemistry analysis of amyloid-β (Aβ) deposition at 4 and 7 months of age in the brain of Treg-depleted or control-treated APPPS1 mice. (**A**) Percentage of area covered by amyloid-β in the cortex and hippocampus. (**B**) Quantification of cortical amyloid-β deposits of different size ranges (0–100; 100–200; 200–500; 500–1000; > 1000 μm^2). (**C**) Brain levels of amyloid-β quantified by ELISA in formic acid-treated insoluble and diethylamine-soluble fractions at 4 months of age. Mean ± SEM (n = 4–6 mice/group). Data representative of two independent experiments. Mann-Whitney test. *$P < 0.05$, **$P < 0.01$. n.s. = not significant.

months of age, i.e. 1 month before the expected onset of cognitive decline in untreated APPPS1 mice. Whereas cognition in PBS-treated APPPS1 was not yet impaired compared to wild-type animals, Treg-depleted APPPS1 mice displayed altered learning abilities, with significantly less accuracy and more total errors searching for the target hole (Fig. 1C). These data suggest that Tregs modulate the kinetics of disease progression in APPPS1 mice by delaying the onset of cognitive deficits.

Treg cell depletion does not alter amyloid-β deposition but decreases plaque-associated microglia in APPPS1 mice

We investigated the impact of early Treg cell depletion on amyloid-β deposition in APPPS1 mice. Whereas an increase in amyloid pathology was observed by immunohistochemistry between 4 and 7 months of age, no difference in total amyloid-β deposition was evident in the cortex or hippocampus of Treg-depleted APPPS1 mice compared to control-treated animals (Fig. 2A). Analysis of size distribution of cortical amyloid deposits also showed similar patterns of amyloid-β deposition in Treg-depleted and non-depleted animals (Fig. 2B). Overall burden of soluble and insoluble amyloid-$\beta_{1–42}$ quantified by ELISA was not significantly different in the brain of Treg-depleted and non-depleted mice (Fig. 2C). These data strongly suggest that transient depletion of Tregs does not alter amyloid deposition in APPPS1 mice, neither in the form of plaques nor as soluble amyloid-β species.

We then evaluated the impact of Treg cell depletion on microgliosis and astrocytosis that are associated with disease progression in APPPS1 mice. Quantification of GFAP-stained surface area showed a significant astrocytosis in the brain of PBS-treated APPPS1 mice as compared to wild-type littermates. Early Treg cell depletion did not alter the extent of GFAP staining in the cortex and hippocampus, neither in APPPS1 nor wild-type mice (Fig. 3A). To evaluate overall microgliosis we first quantified the global brain areas reactive for Iba1 immunostaining. Enhanced Iba1 expression was observed in the cortex and hippocampus of PBS-treated APPPS1 mice as compared to wild-type littermates. Treg cell depletion also did not alter the extent of Iba1 staining in the brain of APPPS1 and wild-type mice (Fig. 3B). Similar results were obtained when analysing the expression of microglial activation marker CD68 (Fig. 3C). To further investigate microglia activation and behaviour, we then evaluated the recruitment of activated microglia towards amyloid plaques by quantifying Iba1 or CD68 staining proximal to amyloid deposits. Although the amount of Iba1 staining co-localizing with or in close vicinity of amyloid-β plaques gradually increases with the size range of amyloid-β deposits in the cortex of both treated and non-treated APPPS1 mice, plaque-associated Iba1 immunoreactivity was markedly decreased in Treg-depleted APPPS1 as compared to non-depleted mice. Recruitment of

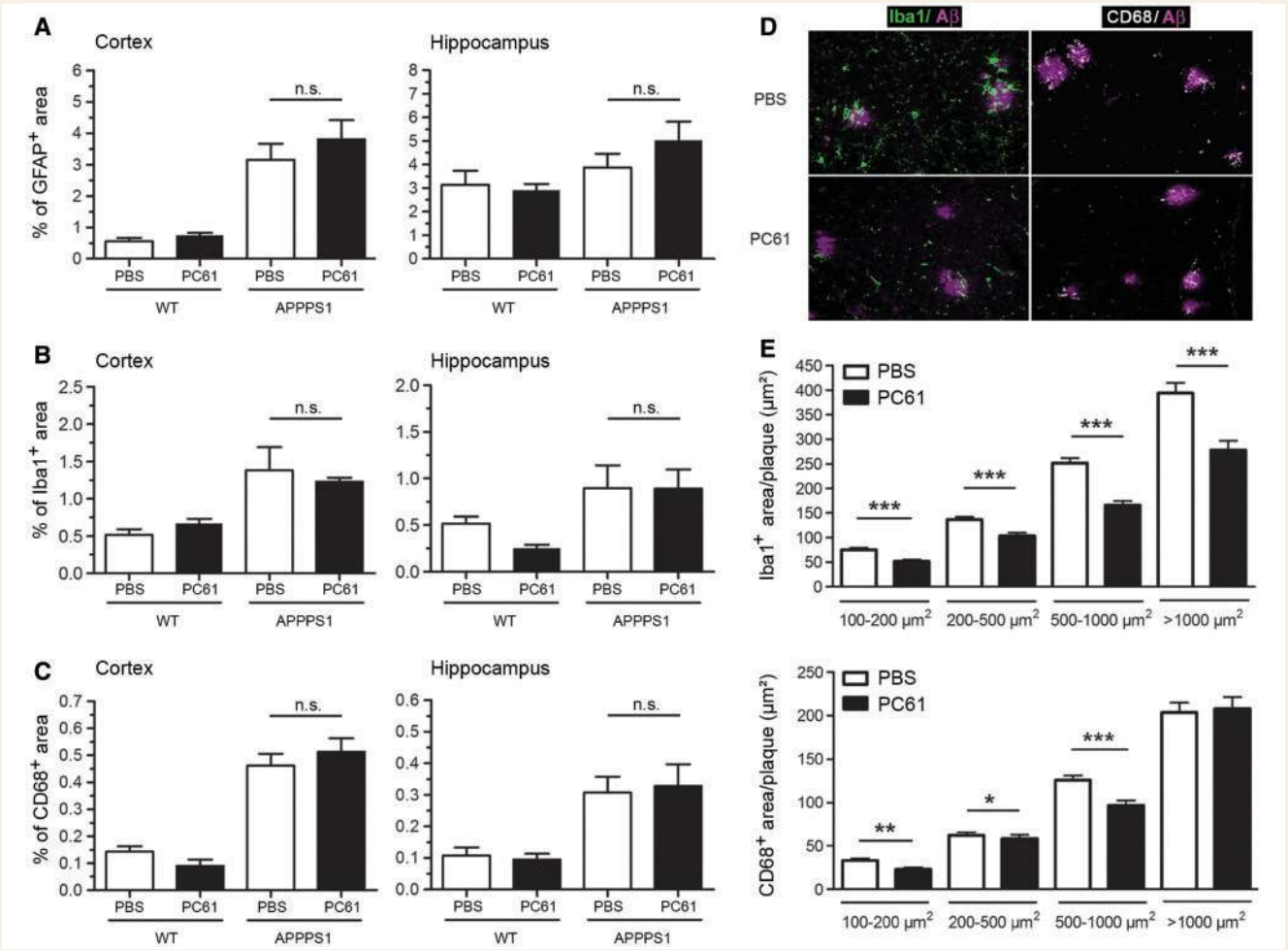

Figure 3 Early depletion of Tregs reduces plaque-associated microglia. (**A**–**C**) Overall extent of astrocytosis, microgliosis, and microglia activation in the cortex and hippocampus of Treg-depleted or non-depleted APPPS1 and wild-type (WT) mice, measured by immunoreactivity to GFAP (**A**), Iba1 (**B**) and CD68 (**C**) at 4 months of age, respectively. Mean ± SEM (n = 4–6 mice/group). (**D** and **E**) Microglia recruitment towards amyloid-β plaques. Representative images (**D**) and quantification (**E**) of Iba1 and CD68 immunoreactivity co-localized with or in close vicinity of cortical amyloid-β (Aβ) deposits of different size ranges. Mean ± SEM ($n > 90$ plaques for each size category; from 4–6 mice/group). Data representative of two independent experiments. Mann-Whitney test. n.s. = non-significant; *$P < 0.05$; **$P < 0.01$; ***$P < 0.001$.

CD68$^+$ microglia towards amyloid-β deposits was also significantly decreased by Treg cell depletion (Fig. 3D and E). Collectively, these data suggest that Treg cell depletion does not alter the overall magnitude of microgliosis or astrocytosis, but significantly reduces the recruitment of activated microglia towards amyloid deposits.

Treg cell depletion alters disease-related gene expression profile in the brain of APPPS1 mice

To gain a broader understanding of the impact of Tregs on disease pathophysiology, we performed gene array analysis. We first compared brain transcriptome of untreated wild-type and APPPS1, which identified a set of 668 genes specifically associated with APPPS1 condition. Such disease-related gene expression profile comprises 387 upregulated and 281 downregulated probes in APPPS1 mice (Fig. 4A and Supplementary Fig. 1A–C). Upregulated transcripts included genes related to astrogliosis, microgliosis and neuroinflammation [*Gfap*, *Aif1*(Iba1), *Cd68*, *Trem2*, *Tyrobp*, *Tspo*, *Tlr2*, *Naip5*, *Ccl3*, *Ccl4*, *Ccl6*, *C1qb*, *C1qc*, *C4a*, *C4b*, *Fcgr2b*, *Ctss*, *Mpeg1*, *Cfs1r*, *Cfs3r*] as well as genes related to type I interferon (IFN) response (*Ifit2*, *Ifit3*, *Ifitm1*, *Ifitm3*). Downregulated genes included receptors for neurotransmitter, neuropeptide and neurotrophic factors (*Gabbr1*, *Gabrg2*, *Ntsr1*, *Ngfr*), regulators of neuronal activity and plasticity [*Camkk2*, *Fkbp1b*, *Khdrbs1*(Sam68)], regulators of dendrite development and synapse maturation (*EphA5*, *EphA7*) and regulators of endocytosis and intracellular vesicle trafficking (*Cav2*, *Rab3b*, *Rab5a*, *Rab6*, *Rab33a*) (Fig. 4A). Using Ingenuity's pathway analysis of downstream effects, we interrogated the APPPS1 versus wild-type gene expression pattern with respect to cellular functions. APPPS1 mice

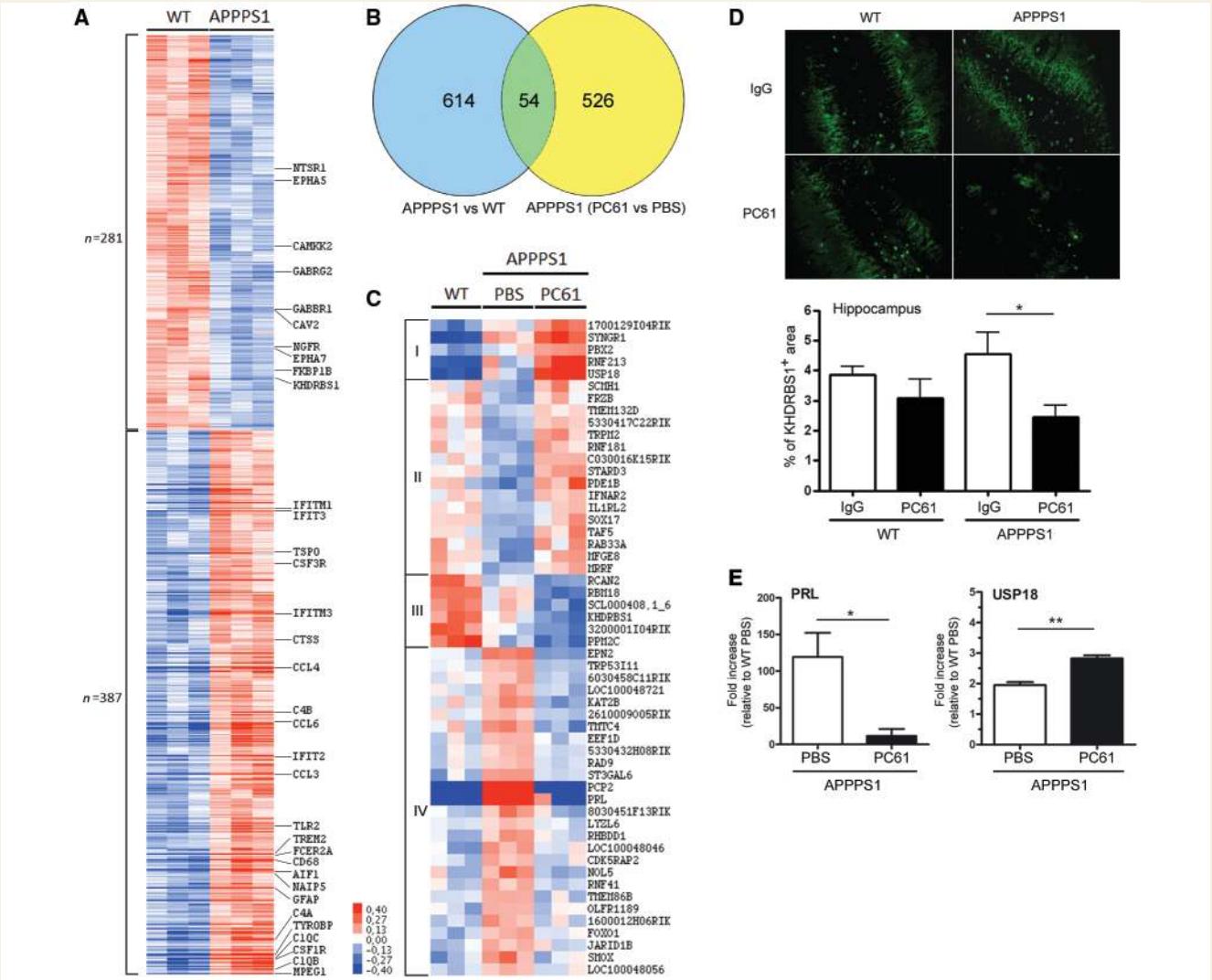

Figure 4 Depletion of Tregs alters disease-related gene expression profile in the brain of APPPS1 mice. (**A**) Heat map of differentially expressed genes in the brain of PBS-treated APPPS1 as compared to wild-type (WT) mice. Each column represents one mouse and each row an individual probe. Genes representative of upregulated and downregulated functions are indicated. (**B**) Venn diagram identifying disease-related genes differentially modulated upon depletion of Tregs. Blue circle represents 668 disease-related probes (APPPS1 versus wild-type) and yellow circle shows 580 treatment-related probes (PC61- versus PBS-treated APPPS1). Green intersection reveals 54 disease-related genes differentially modulated by PC61 treatment. (**C**) Heat map showing the expression profile of 54 disease-related genes differentially modulated upon Treg cell depletion. Each column represents one mouse and each row corresponds to one gene. For all gene array analyses, only genes with significant $P \leqslant 0.05$ and with modulations significantly different and above the background noise modulations (2xSD) are represented. Relative abundance of transcripts is indicated according to colour scale. (**D**) Representative images and quantification of KHDRBS1/SAM68 immunoreactivity in the hippocampus of Treg-depleted or non-depleted wild-type and APPPS1 mice. Mean ± SEM (n = 4–6 mice/group). Mann-Whitney test; $^{*}P < 0.05$. (**E**) Relative quantification by real-time quantitative PCR of *Prl* and *Usp18* mRNA expression in the brain of Treg-depleted and non-depleted APPPS1 mice. Data are expressed as fold increase relative to untreated wild-type mice. Unpaired Student's t-test; $^{*}P < 0.05$; $^{**}P < 0.01$.

showed upregulation of functions mostly associated with migration, recruitment, activation and differentiation of myeloid cells and mononuclear phagocytes, i.e. microglia and/or macrophages. Functions associated with recruitment, viability and activation of lymphocytes and neutrophils were similarly upregulated. Additional functions related to developmental delay, lipid and glucose metabolism, and protein catabolism also tend to be upregulated (Supplementary Fig. 2). Conversely, processes related to nervous system development and functions (development of dendritic spines, regeneration of neurites), behaviour (conditioning, spatial learning, cognition), organization of cytoplasm and cytoskeleton, and cell death and survival tended to be downregulated (Supplementary Fig. 2). In parallel, comparison of the transcriptome from Treg-depleted and non-depleted APPPS1 mice identified 580 probes that were differentially expressed in the brain of APPPS1 animals after Treg cell depletion. Comparative analysis of the

two gene expression profiles, i.e. 668 genes associated with APPPS1 condition and 580 genes associated with depletion of Tregs within APPPS1 mice, was then carried out for identifying overlapping genes. This highlighted a series of 54 disease-related genes, the expression of which was differentially modulated upon Treg cell depletion (Fig. 4B and C). Based on Ingenuity pathway analysis, these genes were associated with multiple processes, including behaviour, nervous system development and functions, cardiovascular system development and functions, inflammatory and cell-mediated immune responses, nucleic acid metabolism, gene expression regulation, lipid metabolism, carbohydrate metabolism, protein synthesis and modification, cell cycle regulation, cell death and survival (Supplementary Fig. 3). Treg cell depletion strengthened the pathological expression profile of 11 disease-related genes that were either further upregulated (Group I) or downregulated (Group III) in the absence of Tregs, suggesting that Tregs may restrain several disease-promoting mechanisms. Among Group I, *Syngr1* codes for the synaptic vesicle protein synaptogyrin 1, which plays an essential role in synaptic plasticity (Janz *et al.*, 1999). *Khdrbs1*/Sam68 (Group III) encodes a key regulator of neuronal activity-dependent alternative splicing, a process playing a central role in circuit assembly and plasticity processes in the brain (Iijima *et al.*, 2011). Our Microarray analysis suggests that deregulated expression of *Syngr1* and *Khdrbs1*/Sam68 observed in APPPS1 mice was further accentuated upon Treg depletion. Although no significant differences in the expression of KHDRBS1/SAM68 (Group III) protein could be detected by immunohistochemistry in the hippocampus of wild-type and APPPS1 mice, expression was significantly decreased in Treg-depleted APPPS1 mice, in line with microarray data (Fig. 4D). Thus, Tregs activity may contribute to mitigate alteration of synaptic plasticity in Alzheimer's disease. Groups II and IV comprise 43 disease-related genes whose pathological expression profile was reverted or normalized upon Treg cell depletion, suggesting a detrimental impact of Tregs in several disease-promoting processes. *Frzb* and *Lrp6* (Group II) are key components of the Wnt/β-catenin canonical pathway, which modulates assembly and function of glutamatergic synapse, as well as positively regulates neurogenesis (Inestrosa and Varela-Nallar, 2014). Expression of *Frzb* and *Lrp6* was downregulated in APPPS1 mice, reminiscent of Wnt pathway alterations observed in Alzheimer's disease (Inestrosa and Varela-Nallar, 2014), but was reverted in Treg-depleted mice. *Foxo1* and *Prl* (Group IV) encode other multifunctional factors that modulate numerous functions and pathways including cell differentiation, stress resistance, metabolism, neurogenesis, proliferation, apoptosis, and vascular functions. Real-time quantitative PCR analysis confirmed that pathological expression profile of *Prl* was reverted in Treg-depleted mice (Fig. 4E). Thus, Tregs may also promote alteration of multifunctional pathways that contribute to disease progression through impaired regulation of synaptic function, cell differentiation and vascular function. Importantly, reversion of pathology-associated pattern in Groups II and IV may also be detrimental, such as for *Ifnar2* coding for type I IFN receptor. Type I IFN response at the choroid plexus was recently shown to negatively affect cognitive functions and hippocampal neurogenesis (Baruch *et al.*, 2014). Disease-related gene expression profile showed active type I interferon response in APPPS1 mice, evidenced by expression of *Ifit* and *Ifitms* genes, despite partial downregulation of *Ifnar2* (Fig. 4A). Reversion towards *Ifnar2* upregulation upon Treg cell depletion may thus be detrimental, suggestive of a possible beneficial inhibitory effect of Tregs on type I interferon response at the choroid plexus. Finally, *Il1rl2* (Group II), the expression of which is reverted from downregulated in APPPS1 mice to upregulated upon Treg cell depletion, codes for IL-36R that displays a particular functional regulation pattern in the brain. It is specifically expressed by microglia and astrocytes, and may contribute to modulate their function (Boraschi and Tagliabue, 2013). Similarly, USP18 has recently been identified as a critical negative regulator of microglia activation through the type I IFN pathway (Goldmann *et al.*, 2015). Microarray data suggest that APPPS1-associated upregulation of *Usp18* was further enhanced in Treg-depleted mice, which was also confirmed by real-time quantitative PCR (Fig. 4E). Thus, the change in expression profile of *Il1rl2* and *Usp18* in APPPS1 mice upon Treg cell depletion may reflect a shift in the functionality of microglial cells, reminiscent of altered microglia recruitment in Treg-depleted mice.

Low-dose IL-2 treatment selectively enhances Treg cell frequency and restores cognitive functions in APPPS1 mice

Our depletion studies suggest that Treg cells play a beneficial role in the pathophysiology of Alzheimer-like pathology and delay disease progression in APPPS1 mice. We therefore investigated the impact of low-dose IL-2 treatment, which was recently described as an efficient strategy for selectively enhancing Treg responses in several pathologies associated with deregulation of Tregs (Grinberg-Bleyer *et al.*, 2010; Koreth *et al.*, 2011; Saadoun *et al.*, 2011; Hartemann *et al.*, 2013; Pilon *et al.*, 2014). Wild-type and APPPS1 mice received daily intraperitoneal injections of either PBS or low doses (50 000 IU/mice/day) of recombinant IL-2 for 10 days, starting at 6 weeks of age, i.e. the age of onset of amyloid-β deposition in this model. Flow cytometry analyses carried out before and 4, 8 and 11 days after the first IL-2 injection revealed enhanced frequency of $CD4^+CD25^+Foxp3^+$ Tregs in the blood of IL-2-treated wild-type and APPPS1 mice (Fig. 5A and B). A similar increase in Tregs was also observed in spleen and cervical lymph nodes after treatment completion (Fig. 5C). In contrast, low-dose IL-2 treatment did not significantly alter the frequency of $CD4^+CD25^+Foxp3^-$ Teffs in the

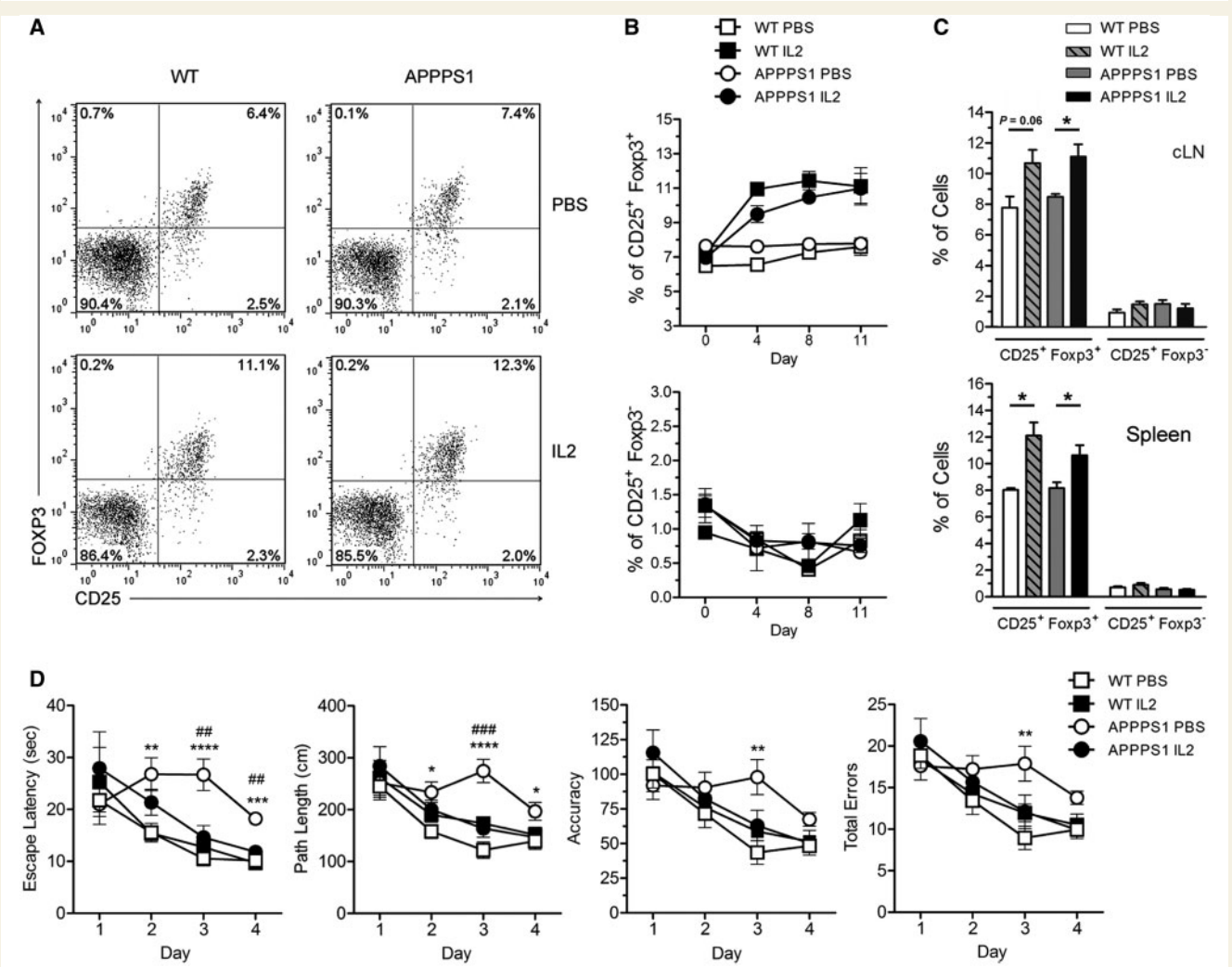

Figure 5 Low-dose IL-2 treatment selectively amplifies Tregs and restores cognitive functions in APPPS1 mice. Six-week-old wild-type (WT) and APPPS1 mice were injected daily intraperitoneally with PBS or 50 000 IU of recombinant human (rh)IL-2 for 10 days. Daily treatments for 5 days were repeated every 3 weeks. (**A–C**) Frequency of $CD25^+Foxp3^+$ Tregs and $CD25^+Foxp3^-$ Teffs among $TCR\beta^+CD4^+$ cells was analysed by flow cytometry. (**A**) Representative dot plots from blood at Day 11 of IL-2 treatment. (**B**) Quantification of Tregs and Teffs in the blood before and after 4, 8 and 11 days of treatment. (**C**) Quantification in spleen and cervical lymph nodes (Day 11). Mean ± SEM (n = 3–4 mice/group). Data representative of two independent experiments. Unpaired Student's t-test. $^*P < 0.05$. (**D**) Impact of IL-2 treatment on spatial learning abilities of 10-month-old wild-type and APPPS1 mice, using the Barnes maze test. Latency, path length, accuracy, and total errors to reach the target hole during the learning phase are shown. Mean ± SEM (n = 9–12 mice/group). Repeated measures ANOVA. $^*P < 0.05$, $^{**}P < 0.01$, $^{***}P < 0.001$, $^{****}P < 0.0001$ versus wild-type PBS; $^{\#\#}P < 0.01$, $^{\#\#\#\#}P < 0.001$ versus APPPS1 IL-2.

blood, spleen, or cervical lymph nodes (Fig. 5A–C). No difference in the total frequency of $CD8^+$ T cells was observed in IL-2-treated mice, and only a non-significant increase in rare $CD8^+CD25^+$ T cell populations was noticed in the spleen, but neither in the blood nor in cervical lymph nodes, of APPPS1 but not wild-type mice (Supplementary Fig. 4A–D). No difference in the percentages of $CD19^+$ B cells and $NK1.1^+$ NK cells was observed (Supplementary Fig. 4E). Thus, low-dose IL-2 treatment selectively enhances the frequency of Tregs in both wild-type and APPPS1 mice, without significantly altering $CD4^+$ Teffs nor other major immune effectors.

The impact of low-dose IL-2 treatment on disease progression was evaluated in chronically IL-2-treated mice. In addition to the initial 10 days of treatment, mice further received daily injections of low-dose IL-2 for 5 days every 3 weeks. Cognitive functions were evaluated at 10 months of age. In the Barnes maze test, PBS-treated APPPS1 mice showed significant impairment in spatial learning compared to PBS-treated wild-type mice, evidenced by less accuracy, more total errors, higher latency and increased path length to reach the target hole. In contrast, no impairment in learning abilities was observed in IL-2-treated APPPS1 mice that behaved similarly to IL-2-treated and untreated wild-type animals (Fig. 5D). Of note, no significant effect of low-dose IL-2 could be detected in APPPS1 mice transiently treated with IL-2 for the first 10 days of treatment only (Supplementary Fig. 5A). Using the Y-maze test, tendency

to beneficial impact of IL-2 treatment on cognitive functions was suggested in both chronically or acutely treated mice, with an apparent stronger effect upon chronic treatment (Supplementary Fig. 5B). Thus, chronic low-dose IL-2 administration restored cognitive functions in a model of Alzheimer-like pathology.

Low-dose IL-2 treatment enhances plaque-associated microglia

We then investigated the impact of chronic low-dose IL-2 treatment on amyloid-β deposition, astrocytosis and microgliosis. A slight non-significant increase in total amyloid-β deposition was observed by immunohistochemistry in the cortex and hippocampus of IL-2-treated APPPS1 mice as compared to control-treated animals (Fig. 6A). Analysis of size distribution of amyloid-β deposits showed similar patterns in the cortex of PBS- or IL-2-treated mice (Fig. 6B). Total load of soluble and insoluble amyloid-β_{1-42} measured by ELISA was also not different in the brain of IL-2- or PBS-treated mice (Fig. 6C). Similarly to amyloid-β deposition, IL-2 treatment slightly but non-significantly increased the overall extent of astrocytosis and microgliosis in APPPS1 mice, as measured by GFAP and Iba1 expression, respectively. No effect was observed in wild-type mice (Fig. 6D and E). No difference in the expression of microglial activation marker CD68 was observed in the brain of IL-2-treated as compared to PBS-treated mice, either wild-type or APPPS1 (Fig. 6F). Nevertheless, conversely to Treg depletion, low-dose IL-2 treatment resulted in a significant increase in plaque-associated Iba1$^+$ and CD68$^+$ cells (Fig. 6G and H). Similar results were obtained when mice received transient instead of chronic IL-2 treatment (Supplementary Fig. 6). Thus, low-dose IL-2 treatment resulted in enhanced microglia recruitment towards amyloid-β deposits.

Discussion

Our study suggests that Tregs play a beneficial role during disease development in a mouse model of Alzheimer-like pathology. Transient depletion of Tregs accelerated the onset of cognitive decline in APPPS1 mice, whereas their amplification resulted in improved learning capacities. Tregs impacted on cognitive functions without altering amyloid-β deposition, but at least in part by modulating microglial response. While overall microgliosis was not significantly affected, depletion of Tregs reduced the recruitment of microglia towards amyloid deposits, whereas their amplification conversely enhanced plaque-associated microglia. Still, neither depletion nor amplification of Tregs impacted on amyloid pathology.

Our results suggest that at least part of the beneficial effect of Tregs we documented is mediated by microglia independently of their amyloid-β-clearing effect. In addition to their phagocytic activity, microglia are known to display multiple other effector functions. They can produce neurotrophic factors and/or inflammatory mediators, regulate neuronal activity by microglia/astrocyte/synapse interactions, as well as contribute to plasticity and synaptic remodelling (Salter and Beggs, 2014). Such functionalities may all contribute to modulate cognitive functions independently of amyloid-β phagocytosis. Accordingly, recent reports in amyloid-transgenic mice showed that potential microglia-derived factors such as BDNF could reverse synapse loss, partially normalize aberrant gene expression, improve cell signalling and restore learning and memory, independently of effects on amyloid deposition (Nagahara *et al.*, 2009). Thus, modulation of selective microglial functions by Treg activity may impact on Alzheimer-related cognitive deficits without altering amyloid clearance. Of note, discrepancies or even inverse correlations between amyloid-β deposition and cognitive deficits have been described in different murine models of amyloid pathology, suggesting that deficits may rather be related to some diffusible amyloid-β species or even intracellular amyloid-β (Duyckaerts *et al.*, 2008). As detailed biochemical characterization of various amyloid-β species was not carried out in our study, we cannot rule out that Treg-mediated effects may also partially relate to altered phagocytic activity of microglia, translating into altered amounts or ratios of given amyloid-β sub-species. Nevertheless, our microarray studies suggest that differential recruitment of Iba1$^+$ cells towards amyloid deposits may reflect a shift in the functionality of resident microglia and/or infiltrating macrophages. Treg depletion in APPPS1 mice modified the expression profile of *Il1rl2*, which is specifically expressed by microglia and astrocytes in the brain, and may modulate their function (Boraschi and Tagliabue, 2013). Similarly, early depletion of Tregs enhanced the expression of Ubiquitin-specific protease 18 (*Usp18*), a critical negative regulator of microglia activation that modulates microglia function by regulating the type I IFN receptor pathway (Goldmann *et al.*, 2015). These data are reminiscent of reduced microglia recruitment in Treg-depleted APPPS1 mice, and suggest that Tregs may contribute to promote a type I IFN-dependent beneficial activation profile of microglia in response to amyloid deposition. Despite being broadly expressed, type I IFN receptor was shown to have a unique protective role on myeloid cells for modulating autoimmune neuroinflammation in the CNS (Prinz *et al.*, 2008). Our data suggest that type I IFNs may help to restrain the development of pro-inflammatory activation profile in microglia at early stages of Alzheimer's disease, thus reducing their possible contribution to impairment of cognitive functions. In the same line, recent report suggested a possible beneficial role of IFNβ1a treatment in patients with early Alzheimer's disease (Grimaldi *et al.*, 2014).

Tregs may modulate the functional differentiation of mononuclear phagocytes through direct interaction within the brain parenchyma. Tregs mediate their suppressive function through several effector mechanisms, including

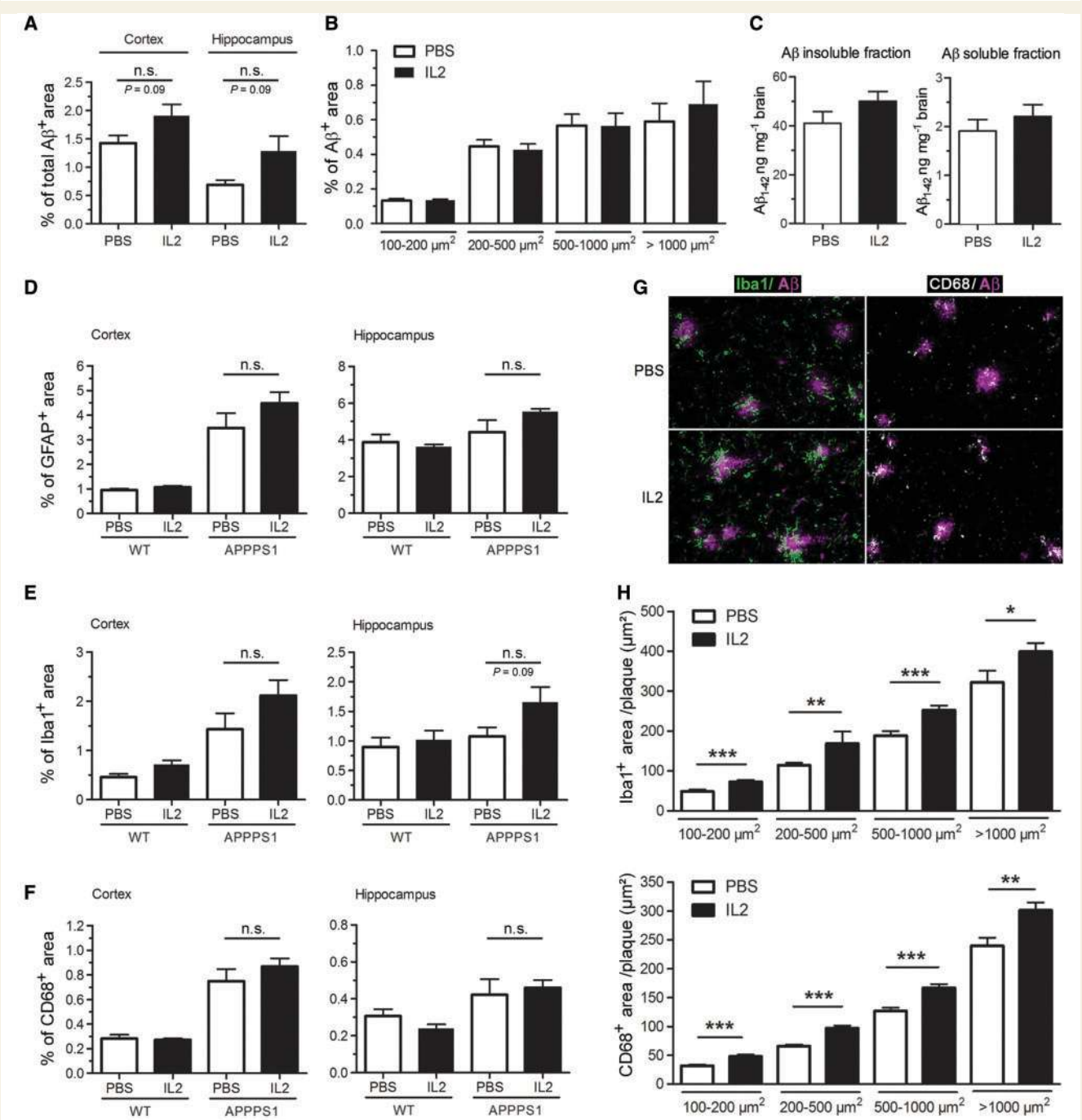

Figure 6 Low-dose IL-2 treatment increases plaque-associated microglia. (**A**) Amyloid-β deposition in the cortex and hippocampus of IL-2- or PBS-treated APPPS1 mice was measured at 4 months of age by immunohistochemistry. (**B**) Quantification of cortical amyloid-β deposits of different size ranges (100–200; 200–500; 500–1000; $>1000\ \mu m^2$). (**C**) Brain levels of amyloid-β were quantified in formic acid-treated insoluble and diethylamine-soluble fractions by ELISA. (**D–F**) Overall extent of astrocytosis, microgliosis, and microglia activation was measured by immunoreactivity to GFAP (**D**), Iba1 (**E**) and CD68 (**F**), respectively. Mean ± SEM (n = 4–6 mice/group). (**G** and **H**) Microglia recruitment towards amyloid-β plaques. Representative images (**G**) and quantification (**H**) of Iba1 and CD68 immunoreactivity co-localized with or in close vicinity of cortical amyloid-β deposits of different size ranges. Mean ± SEM ($n > 90$ plaques for each size category; from 4–6 mice/group). Mann-Whitney test. n.s. = non-significant; $^{*}P < 0.05$; $^{**}P < 0.01$; $^{***}P < 0.001$.

production of immunosuppressive cytokines such as IL-10, TGF-β and IL-35 (Sakaguchi *et al.*, 2008; Shevach, 2009). Whereas recent studies in mouse models of Alzheimer's disease evidenced that IL-10 negatively regulates amyloid-β phagocytosis by microglia, TGF-β has been suggested to promote or mitigate amyloid-β clearance by microglia and peripheral macrophages, respectively (Wyss-Coray *et al.*, 2001; Town *et al.*, 2008; Chakrabarty *et al.*, 2015;

Guillot-Sestier *et al.*, 2015). Although our data suggest that Tregs may contribute to restrain cognitive deficits independently of amyloid-β clearance, further studies will be needed to better decipher the potential role of IL-10, TGF-β and other Treg effector mechanisms in Treg-mediated beneficial effect and functional modulation of microglia activity.

Alternatively, Tregs may alter the recruitment of monocyte-derived macrophages from the periphery to the CNS, fostering infiltration of cells with anti-inflammatory/suppressive activity. The choroid plexus was recently proposed as a selective and educative gate for recruitment of inflammation-resolving leucocytes to the inflamed CNS parenchyma (Schwartz and Baruch, 2014). Type I IFN response at the choroid plexus, in response to brain-derived signals, has been associated with ageing-induced dysfunction of the choroid plexus and cognitive decline (Baruch *et al.*, 2014). Interestingly, our microarray studies evidenced an active type I IFN response associated with APPPS1 condition, as suggested by expression of *Ifit* and *Ifitms* genes. Thus, our data support the hypothesis that brain-derived signals associated with the development of Alzheimer-like pathology may promote choroid plexus dysfunction through a type I IFN-dependent mechanism. However, our Treg depletion studies suggest a more complex implication of type I IFNs in the pathophysiology of Alzheimer's disease, identifying a protective role of Tregs possibly mediated in part by promoting a shift towards type I IFN-dependent beneficial activation profile of microglia. In contrast with our data, a recent report showed that transient depletion of systemic Tregs mitigates Alzheimer-like pathology, by restoring choroid plexus gateway activity in orchestrating the recruitment of inflammation-resolving leucocytes to the CNS. Authors thus concluded to systemic Treg-mediated immunosuppression as being detrimental in Alzheimer's pathology (Baruch *et al.*, 2015). These apparently conflicting results strongly underline the complex role and interplay of Tregs along the course of disease progression. Importantly, a major difference between the two studies is the stage of the disease at which Treg implication was investigated. We evidenced a beneficial role of Tregs by interfering with this immune compartment at early disease stages, when amyloid deposition and gliosis just start developing, i.e. 5–6 weeks of age in our APPPS1 model. In contrast, Baruch and colleagues (2015) modulated peripheral Tregs at an intermediate stage of Alzheimer-like pathology, i.e. 4–5 months of age in the 5XFAD model, after cerebral amyloid-β pathology and gliosis have significantly developed. In this different pathological context, when brain-derived signals arising from amyloid deposition and gliosis have been accumulating for a prolonged period of time, authors show a detrimental impact of Tregs, acting at least in part by reducing choroid plexus ability to recruit leucocytes. Of note, their data further suggest that transient Treg depletion promotes the subsequent recruitment of immunoregulatory cells, including both monocyte-derived macrophages and Tregs, which may then play an active role in mitigating the neuroinflammatory response. Altogether, both studies are consistent with a complex and dual role of Tregs along progression of Alzheimer's pathology. At early disease stages Tregs may contribute to restrain the development of pro-inflammatory gliosis detrimental to cognitive functions, at least in part by promoting type I IFN-dependent beneficial activation profile in microglia. At later disease stages, accumulation of brain-derived signals associated with disease progression may lead to differential conditioning and responsiveness of choroid plexus to Tregs, resulting in Treg-mediated alteration of choroid plexus and impaired recruitment of inflammation-resolving leucocytes to CNS. Alleviating such choroid plexus-related detrimental impact of Tregs may allow fostering again their beneficial effect in mitigating the neuroinflammatory response. Importantly, our data strongly suggest that amplifying Tregs starting from early disease stages may profoundly restrain or even prevent the development of detrimental pro-inflammatory gliosis, and consequently the subsequent choroid plexus responsiveness to Treg-mediated deleterious activity on leucocytes recruitment. Additional studies will be needed for further evaluating this hypothesis and better deciphering the complex interplay of type I IFN and Tregs in the context of Alzheimer's disease.

Functionality of the choroid plexus was shown to be regulated by CNS-specific T cells (Schwartz and Baruch, 2014). We previously showed that Tregs critically control the magnitude of $CD4^+$ Teffs responses to amyloid-β in Alzheimer-like pathology and in response to amyloid-β vaccination (Toly-Ndour *et al.*, 2011). Modulation by Tregs of Teffs responses to amyloid-β may thus contribute to modulate the functionality of choroid plexus epithelium and shape the extent and differentiation profile of macrophages recruited from the periphery. Finally, systemic inflammation was suggested to contribute to exaggerated inflammatory response of primed microglia in neurodegeneration (Perry and Holmes, 2014). Modulation by Tregs of overall systemic inflammatory status may also translate into differential activation and functional differentiation of parenchymal microglia. All such hypotheses are non-mutually exclusive and will need to be addressed in complementary studies.

Our gene array analyses suggest that Tregs may have both beneficial and detrimental impacts on multiple disease-related processes in Alzheimer's disease, pertaining to microglia, type I IFN response and choroid plexus, but also to neuronal activity and vascular functions. As gene array data derive from rather small sample sizes they are thus merely indicative of potential modes of action. The main primary processes directly affected by Tregs, as well as downstream secondary effects, still remain to be further investigated. Nevertheless, overall balance of the effects of Tregs on disease pathophysiology appears beneficial in our study, and boosting Tregs at early disease stages via peripheral administration of low-dose IL-2 restores cognitive functions in Alzheimer-like pathology. Of note, whereas a

beneficial effect of low-dose IL-2 treatment was observed for chronically treated APPPS1 mice, only a tendency towards improved cognition was suggested in transiently treated animals. These data suggest that transient low-dose IL-2 treatment may be sufficient for initiating Treg-mediated beneficial processes, but recurrent or sustained amplification of Tregs starting from early disease stages seems necessary for fully supporting the entire neuroprotective effect. Importantly, low-dose IL-2 treatment was shown to be clinically well tolerated and efficient at modulating Treg responses in several human pathological settings (Koreth *et al.*, 2011; Saadoun *et al.*, 2011; Hartemann *et al.*, 2013). These promising preliminary studies strongly support further clinical assessment of low-dose IL-2 treatment in inflammatory diseases, and underline the high potential for rapid translation to clinical trials (Klatzmann and Abbas, 2015). Our proof-of-concept preclinical study in a mouse model of Alzheimer-like pathology suggests that such Treg-based immunomodulatory approaches may constitute innovative therapeutic and even preventive strategies for slowing cognitive decline and disease progression in Alzheimer's disease.

Acknowledgements

We thank Dr Benoit Delatour and Dr Thomas Freret for expert discussions on mouse behaviour experiments, Tatiana Ledent and the staff of PHEA for dedicated assistance with mouse husbandry, and Anne-Marie Faussat and Annie Munier from the LUMIC flow cytometry facility.

Funding

This work was supported by grants from Association France Alzheimer, Fondation de France, LECMA, Fondation Plan Alzheimer, INSERM, Université Pierre et Marie Curie, and Institut de Neurosciences translationnelles de Paris (IHU-A-ICM).

Supplementary material

Supplementary material is available at *Brain* online.

References

Baruch K, Deczkowska A, David E, Castellano JM, Miller O, Kertser A, et al. Aging-induced type I interferon response at the choroid plexus negatively affects brain function. Science 2014; 346: 89–93.

Baruch K, Rosenzweig N, Kertser A, Deczkowska A, Sharif AM, Spinrad A, et al. Breaking immune tolerance by targeting Foxp3(+) regulatory T cells mitigates Alzheimer's disease pathology. Nat Commu 2015; 6: 7967.

Beers DR, Henkel JS, Zhao W, Wang J, Huang A, Wen S, et al. Endogenous regulatory T lymphocytes ameliorate amyotrophic lateral sclerosis in mice and correlate with disease progression in patients with amyotrophic lateral sclerosis. Brain 2011; 134 (Pt 5): 1293–314.

Boraschi D, Tagliabue A. The interleukin-1 receptor family. Semin Immunol 2013; 25: 394–407.

Cao C, Arendash GW, Dickson A, Mamcarz MB, Lin X, Ethell DW. Aβ-specific Th2 cells provide cognitive and pathological benefits to Alzheimer's mice without infiltrating the CNS. Neurobiol Dis 2009; 34: 63–70.

Chakrabarty P, Li A, Ceballos-Diaz C, Eddy JA, Funk CC, Moore B, et al. IL-10 alters immunoproteostasis in APP mice, increasing plaque burden and worsening cognitive behavior. Neuron 2015; 85: 519–33.

Duyckaerts C, Potier MC, Delatour B. Alzheimer disease models and human neuropathology: similarities and differences. Acta Neuropathol 2008; 115: 5–38.

Ethell DW, Shippy D, Cao C, Cracchiolo JR, Runfeldt M, Blake B, et al. Aβ-specific T-cells reverse cognitive decline and synaptic loss in Alzheimer's mice. Neurobiol Dis 2006; 23: 351–61.

Ferrer I, Boada Rovira M, Sanchez Guerra ML, Rey MJ, Costa-Jussa F. Neuropathology and pathogenesis of encephalitis following amyloid-beta immunization in Alzheimer's disease. Brain Pathol 2004; 14: 11–20.

Goldmann T, Zeller N, Raasch J, Kierdorf K, Frenzel K, Ketscher L, et al. USP18 lack in microglia causes destructive interferonopathy of the mouse brain. EMBO J 2015; 34: 1612–29.

Grimaldi LM, Zappala G, Iemolo F, Castellano AE, Ruggieri S, Bruno G, et al. A pilot study on the use of interferon beta-1a in early Alzheimer's disease subjects. J Neuroinflammation 2014; 11: 30.

Grinberg-Bleyer Y, Baeyens A, You S, Elhage R, Fourcade G, Gregoire S, et al. IL-2 reverses established type 1 diabetes in NOD mice by a local effect on pancreatic regulatory T cells. J Exp Med 2010; 207: 1871–8.

Guillot-Sestier MV, Doty KR, Gate D, Rodriguez J Jr, Leung BP, Rezai-Zadeh K, et al. Il10 deficiency rebalances innate immunity to mitigate Alzheimer-like pathology. Neuron 2015; 85: 534–48.

Hartemann A, Bensimon G, Payan CA, Jacqueminet S, Bourron O, Nicolas N, et al. Low-dose interleukin 2 in patients with type 1 diabetes: a phase 1/2 randomised, double-blind, placebo-controlled trial. Lancet Diabetes Endocrinol 2013; 1: 295–305.

Iijima T, Wu K, Witte H, Hanno-Iijima Y, Glatter T, Richard S, et al. SAM68 regulates neuronal activity-dependent alternative splicing of neurexin-1. Cell 2011; 147: 1601–14.

Inestrosa NC, Varela-Nallar L. Wnt signaling in the nervous system and in Alzheimer's disease. J Mol Cell Biol 2014; 6: 64–74.

Janus C, Pearson J, McLaurin J, Mathews PM, Jiang Y, Schmidt SD, et al. A beta peptide immunization reduces behavioural impairment and plaques in a model of Alzheimer's disease. Nature 2000; 408: 979–82.

Janz R, Sudhof TC, Hammer RE, Unni V, Siegelbaum SA, Bolshakov VY. Essential roles in synaptic plasticity for synaptogyrin I and synaptophysin I. Neuron 1999; 24: 687–700.

Jones L, Holmans PA, Hamshere ML, Harold D, Moskvina V, Ivanov D, et al. Genetic evidence implicates the immune system and cholesterol metabolism in the aetiology of Alzheimer's disease. PLoS One 2010; 5: e13950.

Klatzmann D, Abbas AK. The promise of low-dose interleukin-2 therapy for autoimmune and inflammatory diseases. Nat Rev Immunol 2015; 15: 283–94.

Koreth J, Matsuoka K, Kim HT, McDonough SM, Bindra B, Alyea EP III, et al. Interleukin-2 and regulatory T cells in graft-versus-host disease. N Engl J Med 2011; 365: 2055–66.

Lambert JC, Grenier-Boley B, Chouraki V, Heath S, Zelenika D, Fievet N, et al. Implication of the immune system in Alzheimer's disease: evidence from genome-wide pathway analysis. J Alzheimers Dis 2010; 20: 1107–18.

Lambert JC, Ibrahim-Verbaas CA, Harold D, Naj AC, Sims R, Bellenguez C, et al. Meta-analysis of 74 046 individuals identifies 11 new susceptibility loci for Alzheimer's disease. Nat Genet 2013; 45: 1452–8.

Larbi A, Pawelec G, Witkowski JM, Schipper HM, Derhovanessian E, Goldeck D, et al. Dramatic shifts in circulating CD4 but not CD8 T cell subsets in mild Alzheimer's disease. J Alzheimers Dis 2009; 17: 91–103.

Monsonego A, Imitola J, Petrovic S, Zota V, Nemirovsky A, Baron R, et al. Abeta-induced meningoencephalitis is IFN-gamma-dependent and is associated with T cell-dependent clearance of Abeta in a mouse model of Alzheimer's disease. Proc Natl Acad Sci USA 2006; 103: 5048–53.

Monsonego A, Zota V, Karni A, Krieger JI, Bar-Or A, Bitan G, et al. Increased T cell reactivity to amyloid beta protein in older humans and patients with Alzheimer disease. J Clin Invest 2003; 112: 415–22.

Morgan D, Diamond DM, Gottschall PE, Ugen KE, Dickey C, Hardy J, et al. A beta peptide vaccination prevents memory loss in an animal model of Alzheimer's disease. Nature 2000; 408: 982–5.

Nagahara AH, Merrill DA, Coppola G, Tsukada S, Schroeder BE, Shaked GM, et al. Neuroprotective effects of brain-derived neurotrophic factor in rodent and primate models of Alzheimer's disease. Nat Med 2009; 15: 331–7.

Nicoll JA, Wilkinson D, Holmes C, Steart P, Markham H, Weller RO. Neuropathology of human Alzheimer disease after immunization with amyloid-beta peptide: a case report. Nat Med 2003; 9: 448–52.

Orgogozo JM, Gilman S, Dartigues JF, Laurent B, Puel M, Kirby LC, et al. Subacute meningoencephalitis in a subset of patients with AD after Abeta42 immunization. Neurology 2003; 61: 46–54.

Perry VH, Holmes C. Microglial priming in neurodegenerative disease. Nat Rev Neurol 2014; 10: 217–24.

Pilon CB, Petillon S, Naserian S, Martin GH, Badoual C, Lang P, et al. Administration of low doses of IL-2 combined to rapamycin promotes allogeneic skin graft survival in mice. Am J Transplant 2014; 14: 2874–82.

Prinz M, Schmidt H, Mildner A, Knobeloch KP, Hanisch UK, Raasch J, et al. Distinct and nonredundant in vivo functions of IFNAR on myeloid cells limit autoimmunity in the central nervous system. Immunity 2008; 28: 675–86.

Reynolds AD, Stone DK, Hutter JA, Benner EJ, Mosley RL, Gendelman HE. Regulatory T cells attenuate Th17 cell-mediated nigrostriatal dopaminergic neurodegeneration in a model of Parkinson's disease. J Immunol 2010; 184: 2261–71.

Rosenkranz D, Weyer S, Tolosa E, Gaenslen A, Berg D, Leyhe T, et al. Higher frequency of regulatory T cells in the elderly and increased suppressive activity in neurodegeneration. J Neuroimmunol 2007; 188: 117–27.

Saadoun D, Rosenzwajg M, Joly F, Six A, Carrat F, Thibault V, et al. Regulatory T-cell responses to low-dose interleukin-2 in HCV-induced vasculitis. N Engl J Med 2011; 365: 2067–77.

Sakaguchi S, Yamaguchi T, Nomura T, Ono M. Regulatory T cells and immune tolerance. Cell 2008; 133: 775–87.

Salter MW, Beggs S. Sublime microglia: expanding roles for the guardians of the CNS. Cell 2014; 158: 15—24.

Saresella M, Calabrese E, Marventano I, Piancone F, Gatti A, Calvo MG, et al. PD1 negative and PD1 positive CD4+ T regulatory cells in mild cognitive impairment and Alzheimer's disease. J Alzheimers Dis 2010; 21: 927–38.

Schenk D, Barbour R, Dunn W, Gordon G, Grajeda H, Guido T, et al. Immunization with amyloid-beta attenuates Alzheimer-disease-like pathology in the PDAPP mouse. Nature 1999; 400: 173–7.

Schwartz M, Baruch K. The resolution of neuroinflammation in neurodegeneration: leukocyte recruitment via the choroid plexus. EMBO J 2014; 33: 7–22.

Shevach EM. Mechanisms of foxp3+ T regulatory cell-mediated suppression. Immunity 2009; 30: 636–45.

Togo T, Akiyama H, Iseki E, Kondo H, Ikeda K, Kato M, et al. Occurrence of T cells in the brain of Alzheimer's disease and other neurological diseases. J Neuroimmunol 2002; 124: 83–92.

Toly-Ndour C, Lui G, Nunes MM, Bruley-Rosset M, Aucouturier P, Dorothee G. MHC-independent genetic factors control the magnitude of CD4+ T cell responses to amyloid-beta peptide in mice through regulatory T cell-mediated inhibition. J Immunol 2011; 187: 4492–500.

Town T, Laouar Y, Pittenger C, Mori T, Szekely CA, Tan J, et al. Blocking TGF-beta-Smad2/3 innate immune signaling mitigates Alzheimer-like pathology. Nat Med 2008; 14: 681–7.

Wyss-Coray T, Lin C, Yan F, Yu GQ, Rohde M, McConlogue L, et al. TGF-beta1 promotes microglial amyloid-beta clearance and reduces plaque burden in transgenic mice. Nat Med 2001; 7: 612–18.